Precambrian Research 300 (2017) 168–180

Contents lists available at ScienceDirect

Precambrian Research

journal homepage: www.elsevier.com/locate/precamres

Linking Olympic Dam and the Cariewerloo Basin: Was a sedimentary basin involved in formation of the world's largest uranium deposit?

Alexander R. Cherry[a,*], Jocelyn McPhie[a], Vadim S. Kamenetsky[a], Kathy Ehrig[b], John L. Keeling[c], Maya B. Kamenetsky[a], Sebastien Meffre[a], Olga B. Apukhtina[a]

[a] ARC Centre of Excellence in Ore Deposits (CODES), School of Physical Sciences, University of Tasmania, Hobart, Tasmania 7001, Australia
[b] BHP Billiton Olympic Dam, 55 Grenfell Street, Adelaide, South Australia 5000, Australia
[c] Geological Survey of South Australia, Department of State Development, Adelaide, South Australia 5000, Australia

ARTICLE INFO

Keywords:
Olympic Dam
Sedimentary basin
Pandurra Formation
Cariewerloo Basin
Uranium

ABSTRACT

The supergiant Olympic Dam Cu-U-Au-Ag deposit is hosted by the Olympic Dam Breccia Complex within a ca. 1.59 Ga granite. The breccia complex is largely granite-derived but also includes volcanic clasts and domains of bedded clastic facies. Recently discovered quartz-rich sandstone has a provenance that included Paleoproterozoic and Archean units represented by zircon populations centered at ca. 2.4 Ga and ca. 1.7 Ga. The texture, detrital and cement mineralogy, and distribution of detrital zircon ages in the quartz-rich sandstone closely match those in sandstone of the Pandurra Formation deposited in the regionally extensive intracratonic Cariewerloo Basin (ca. 1.44 Ga). The age of authigenic apatite (1.44 ± 0.02 Ga) in the brecciated quartz-rich sandstone is equivalent to the minimum depositional age of the Pandurra Formation. We conclude that the quartz-rich sandstone is a remnant of the Pandurra Formation, that the Pandurra Formation originally extended across the Olympic Dam Breccia Complex, and that it was incorporated by tectonic activity at least 150 myr after initial formation of the breccia complex. Furthermore, we speculate that oxidized U-bearing fluids from the overlying Cariewerloo Basin may have interacted with the Olympic Dam U resource, consistent with mounting evidence for substantial post-1.59 Ga remobilization and probable addition of U.

1. Introduction

The supergiant Olympic Dam (OD) Cu-U-Au-Ag deposit (10.1 Gt @ 0.78% Cu, 0.25 kg/t U_3O_8, 0.3 g/t Au, 1 g/t Ag; BHP Billiton, 2016) is one of the largest known accumulations of metals, particularly U (Reeve et al., 1990; Ehrig et al., 2012). Olympic Dam is regarded as the flagship of the IOCG (iron-oxide-copper-gold) deposit class (Hitzman et al., 1992), although OD is distinct by virtue of its size and being the only deposit of this class to have economic quantities of U (Hitzman and Valenta, 2005).

The OD deposit is hosted by a breccia complex (Olympic Dam Breccia Complex, ODBC) within the ca. 1.59 Ga Roxby Downs Granite (RDG). Although early research concluded that OD was an unusual type of sediment-hosted Cu deposit (Roberts and Hudson, 1983), later research has favored a hydrothermal origin and close link to a regional magmatic event at ~1.59 Ga (Oreskes and Einaudi, 1990; Reeve et al., 1990; Johnson and Cross, 1995; Skirrow et al., 2007). In addition, the ODBC is now recognized to be multi-stage and hydrothermal-tectonic in origin (Oreskes and Einaudi, 1990; Reeve et al., 1990; McPhie et al., 2011).

The timing of formation of the ODBC is of paramount importance in constraining the timing of OD ore deposition and processes of ore genesis. Until recently, all of the lithological components of the ODBC (granite clasts, volcanic clasts, bedded clastic facies) have returned ages of ca. 1.59 Ga (Johnson and Cross, 1995; Jagodzinski et al., 2014) and the brecciation that generated the ODBC has been considered to have taken place at around the same time (Reeve et al., 1990; Johnson and Cross, 1995). However, McPhie et al. (2016) reported the presence of a brecciated quartz-rich sandstone in the ODBC that has a distinctive detrital zircon age population and provenance. Here we present additional data on the context, texture, mineralogy, petrography, detrital zircon population and diagenetic age of the quartz-rich sandstone. We test the hypothesis that the quartz-rich sandstone is not the same age as the other lithological components of the ODBC (i.e. ca. 1.59 Ga), but is related to other, potentially younger sedimentary formations in the vicinity of OD. The close correlation demonstrated with one of these successions indicates that it once directly overlay the ODBC and that tectonic activity affected the ODBC ~150 myr after initial formation.

* Corresponding author.
E-mail address: alexander.cherry@utas.edu.au (A.R. Cherry).

http://dx.doi.org/10.1016/j.precamres.2017.08.002
Received 7 December 2016; Received in revised form 26 July 2017; Accepted 2 August 2017
Available online 12 August 2017
0301-9268/ © 2017 Elsevier B.V. All rights reserved.

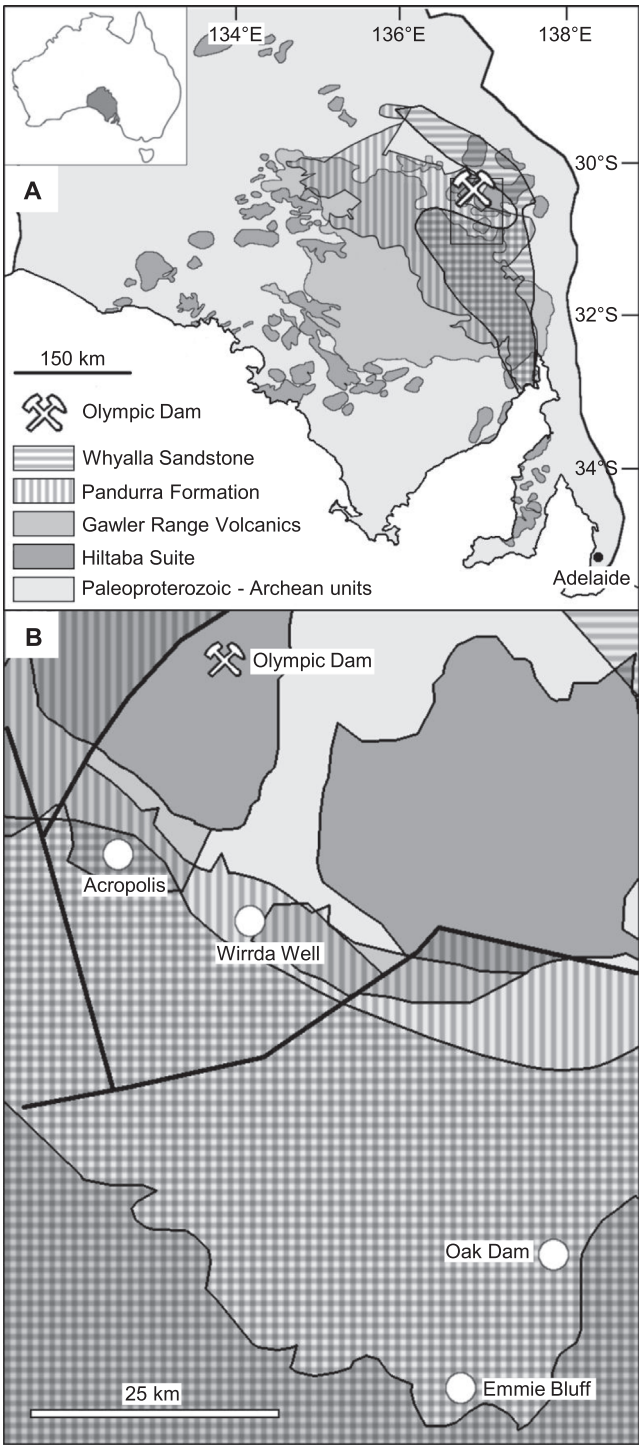


Fig. 1. A: Location of Olympic Dam in the Gawler Craton (after Drexel et al., 1993; McPhie et al., 2011). The map also shows the distribution of the Mesoproterozoic Pandurra Formation and the Neoproterozoic Whyalla Sandstone. Shaded area on the inset map shows the Gawler Craton in South Australia. B: Location of Acropolis, Emmie Bluff, Oak Dam and Wirrda Well IOCG prospects.

Furthermore, we speculate that this allowed access (into the ODBC) of basinal fluids that had the capacity to modify and even upgrade the OD U resource after 1.59 Ga.

2. Regional setting

Olympic Dam is one of several IOCG deposits and prospects in the Olympic IOCG Province along the eastern margin of the Gawler Craton (Skirrow et al., 2007) (Fig. 1). The Gawler Craton comprises Mesoarchean to Paleoproterozoic deformed and metamorphosed lithologies overlain by largely undeformed and unmetamorphosed Mesoproterozoic igneous rocks (Hand et al., 2007). The Mesoproterozoic igneous rocks include the Gawler Range Volcanics (GRV; ca. 1.595–1.587 Ga) (Jagodzinski et al., 2016) and the Hiltaba Suite granitoids, which together constitute the voluminous Gawler Silicic Large Igneous Province (Gawler SLIP) (Allen et al., 2008). The RDG (ca. 1593 Ma; Jagodzinski et al., 2014), which hosts the ODBC, is a member of the Hiltaba Suite (Fig. 1).

The eastern side of the Gawler Craton is unconformably overlain by the mostly flat-lying Mesoproterozoic Pandurra Formation (mainly quartz sandstone) (Cowley, 1993). The Pandurra Formation occurs to the north, west and south of OD (including at the Acropolis, Emmie Bluff, Oak Dam and Wirrda Well IOCG prospects; Fig. 1B) but not at OD (Cowley, 1993). The Pandurra Formation and OD are unconformably overlain by flat-lying Neoproterozoic to Cambrian sedimentary formations (~350 m thick over the ODBC) of the Stuart Shelf (Roberts and Hudson, 1983; Preiss, 1993). The Stuart Shelf succession includes the extensive Neoproterozoic Whyalla Sandstone (Preiss, 1987), which is not preserved, or was not deposited, over the ODBC, but is present over the Acropolis and Emmie Bluff IOCG prospects (Fig. 1B). The Gairdner Dyke Swarm (ca. 0.83 Ga) (Wingate et al., 1998) intruded the Pandurra Formation (Cowley, 1993) and older units in the northeastern Gawler Craton, including the ODBC (Huang et al., 2015).

3. Olympic Dam deposit geology

The ODBC is surrounded by unbrecciated, weakly sericite-altered to fresh RDG and mainly consists of variably altered clasts of the RDG. Hydrothermally altered, brecciated GRV, bedded clastic facies and mafic dykes are locally abundant (Reeve et al., 1990; McPhie et al., 2011; Ehrig et al., 2012). The brecciated GRV records the presence of GRV lavas above the RDG at OD prior to formation of the ODBC (McPhie et al., 2011; Ehrig et al., 2012). The bedded clastic facies occur in large domains with faulted and/or brecciated contacts and as dispersed clasts. The domains and clasts consist of well-bedded mudstone, sandstone and conglomerate, and laminated ironstone (McPhie et al., 2016).

The intensity of hydrothermal alteration and brecciation increases towards the center of the ODBC resulting in a continuum in breccia texture and composition from peripheral sericite-altered, granite-rich breccia to hematite-rich breccia in the center (Reeve et al., 1990; Ehrig et al., 2012). Several sets of steeply dipping brittle faults have been identified in the ODBC; these faults were in place pre- and syn-mineralization and locally show signs of post-mineralization reactivation (Fig. 2) (Ehrig et al., 2012).

The majority of the OD ore minerals are disseminated and show a strong association with the hematite-rich breccia. Copper sulfide minerals (chalcopyrite, bornite and chalcocite-group) are broadly zoned from S-poor sulfides (bornite + chalcocite) to Fe-rich sulfides (pyrite + chalcopyrite) with increasing depth (Reeve et al., 1990). The distribution of U minerals (uraninite + coffinite + brannerite) in the deposit is complex and not obviously zoned (Ehrig et al., 2012). Textures of the U minerals suggest there have been multiple episodes of precipitation and dissolution of U phases (Macmillan et al., 2016).

4. Quartz-rich sandstone in the ODBC

Brecciated quartz-rich sandstone is a very minor component of the ODBC and has been identified in only two drill holes (Fig. 2) (McPhie et al., 2016). In both drill holes, the ~80-m-thick intervals of brecciated quartz-rich sandstone comprise mm- to decimeter-sized fragments of sandstone dispersed in red-brown, hematite-rich sandy matrix (Fig. 3A-C). In vertical drill hole RD1628, the interval of brecciated quartz-rich sandstone is immediately below the unconformity with the

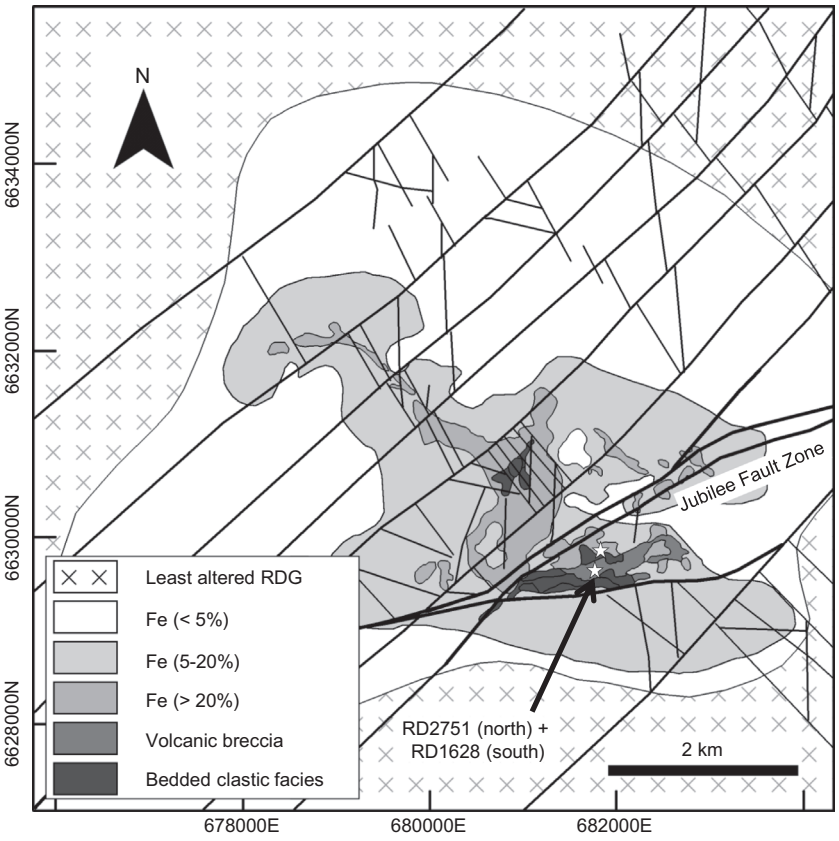


Fig. 2. Map of Olympic Dam Breccia Complex (ODBC) at −350 mRL (after Hayward and Skirrow, 2010; Ehrig et al., 2012; Clark et al., 2016) and collars of RD1628 and RD2751 (stars). Granite breccia in the ODBC is shaded gray relative to Fe content (< 5 wt%, 5–20 wt %, > 20 wt%), volcanic breccia and bedded clastic facies are shaded darker gray. Fault traces are shown as black lines, including the eastnortheast striking Jubilee Fault Zone.

overlying Neoproterozoic succession and has a lower faulted contact with bedded clastic facies (Fig. 4). In inclined drill hole RD2751, the interval of brecciated quartz-rich sandstone is over 400 m below the unconformity surface and has upper and lower faulted contacts with hematite-rich breccia of the ODBC (Fig. 4). The interval of brecciated quartz-rich sandstone in RD2751 is situated below and ~100 m to the east of the interval in RD1628.

The quartz-rich sandstone fragments are angular to rounded (Fig. 3A-C). They are either internally massive or show well-defined internal bedding; the beds are planar or cross-stratified. The sandstone is poorly sorted, and mostly composed of fine- to very coarse-grained, angular to sub-rounded quartz grains with abundant syntaxial quartz overgrowths (Fig. 5A, B). Quartz grains are monocrystalline and polycrystalline; many grains show undulose extinction and contain abundant fluid and mineral inclusions. Minor clastic components include lithic fragments, muscovite, zircon, tourmaline, Ti-oxide (rutile/anatase), hematite and ilmenite. Some samples have abundant lithic clasts. The sandstone is cemented by the quartz overgrowths, and the intraclast pore space is filled mostly by illite/muscovite, and rarely by chlorite (clay speciation determined using reflectance spectroscopy, see supplementary methods and data) and late-stage quartz. Very fine-grained (ca. 10 μm), bladed hematite coats both detrital grains and quartz overgrowths, and is disseminated throughout the cement. Apatite is a minor component observed in the pore cement of a few sandstone fragments as isolated grains that are between 10–100 μm and commonly euhedral or clusters of grains that can be over 200 μm (Fig. 6A). The distribution and grain shape of the apatite suggests it is an authigenic phase. The intergrowth of apatite with the bladed hematite and quartz overgrowths further supports an authigenic origin (see figures in supplementary data).

The red-brown matrix surrounding the sandstone fragments comprises very poorly sorted, very fine- to coarse-grained quartz grains that are generally more angular and irregular (in some cases, embayed) than quartz grains in the sandstone fragments (Fig. 5C). Quartz overgrowths are less common and in many cases have been truncated at grain boundaries. Minor clastic components in the matrix include lithic particles, muscovite, tourmaline and Ti-oxide, similar to those observed in the sandstone fragments. The cement is primarily illite; disseminated very fine-grained, bladed hematite and Ti-oxide are also present. There are small patches of matrix and haloes around sandstone fragments where the cement in the matrix is devoid of hematite (Fig. 5D).

Sulfides, and U and rare earth element (REE) minerals are rare in the brecciated quartz-rich sandstone, as indicated also in drill hole assays which show that economic elements (e.g. U) are mostly below detection (Fig. 4, see supplementary data). Rare chalcopyrite occurs with chlorite in some sandstone fragments; xenotime, thorite, monazite, bastnäsite and synchysite are present only in trace abundances. In contrast, adjacent lithologies have elevated concentrations of Cu, U and REE, characteristic of the OD orebody (Fig. 4).

5. Zircon and apatite geochronology

In order to constrain the regional affinities of the quartz-rich sandstone in the ODBC, we examined the age profile of detrital zircons within the sandstone fragments and determined the age of authigenic apatite in the sandstone matrix.

5.1. Methods

5.1.1. Zircon

Sandstone samples were crushed, sieved and panned to produce a heavy mineral concentrate. After removal of the magnetic fraction with an NdFeB hand magnet, zircons were handpicked and mounted on 1-inch epoxy resin disks and polished. The potential introduction of bias to the detrital zircon age populations through either heavy liquid- or water-based techniques was determined by Sláma and Košler (2012) to mostly occur as preferential loss of smaller zircon grains for both techniques. Mitigation of the tendency to favor larger grains during

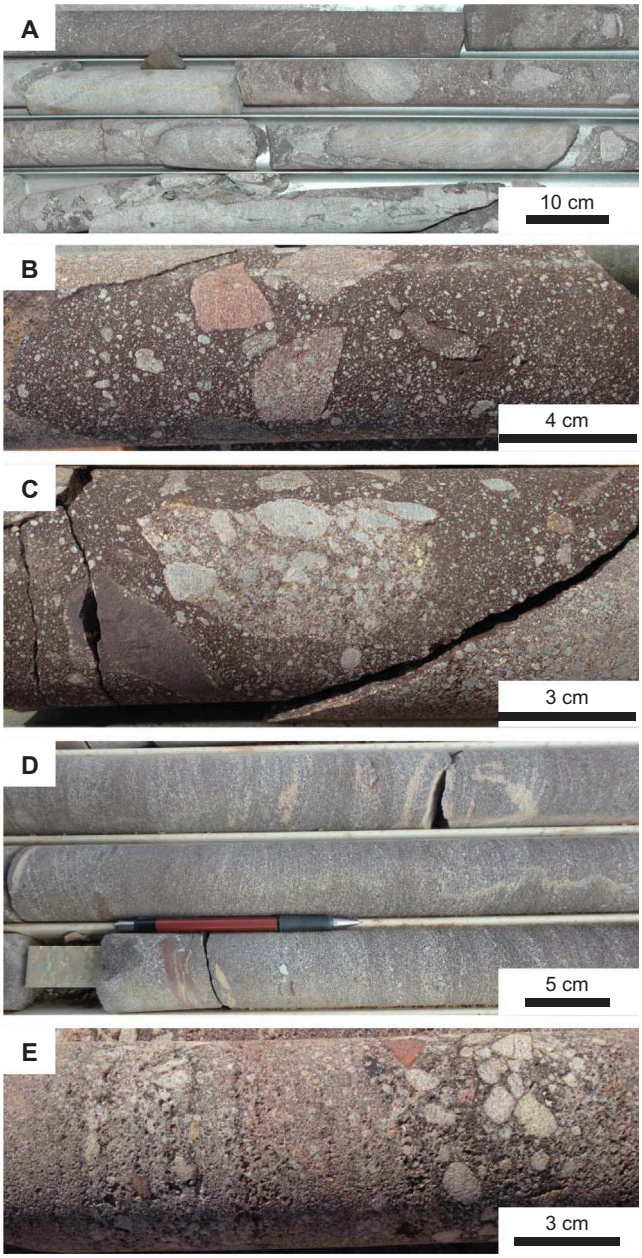


Fig. 3. A: Interval of quartz-rich sandstone fragments in red-brown matrix, RD2751, ~890 m. B, C: Clasts of coarse-grained and pebbly quartz-rich sandstone in red-brown matrix, RD1628, 346.6 m, 352.3 m. D: Interval of Pandurra Formation quartz sandstone above the Acropolis prospect, ACD15, ~480 m. E: Pandurra Formation pebbly coarse sandstone above the Oak Dam prospect, AD3, 537.5 m.

handpicking was attempted through use of a very fine titanium needle to pick grains (instead of tweezers) (e.g. Sláma and Košler, 2012).

Zircons were analyzed using Laser Ablation-Inductively Coupled Mass Spectrometry (LA-ICPMS) at the University of Tasmania (see supplementary method for details of instrument configuration). Age calculations and probability density plots were derived using the program ISOPLOT (Ludwig, 2008). The reference zircon 91500 (Wiedenbeck et al., 1995) was used as a primary standard for all analyses, and additional verification involved the secondary zircon standards Temora (Black et al., 2003), Mud Tank (Black and Gulson, 1978), Plešovice (Sláma et al., 2008) and occasionally JG1 (Jackson et al., 2004) and Qinghu (Li et al., 2013).

The quartz-rich sandstone detrital zircon analyses presented here build on the dataset of McPhie et al. (2016), which was exclusively on samples from drill hole RD2751. In this study, additional samples from drill holes RD2751 as well as RD1628 were analyzed (see supplementary data). The detrital zircon analyses for samples of the other bedded clastic facies are the same as those presented in McPhie et al. (2016). Detrital zircons from two quartz-rich sandstone successions in the vicinity of OD, the Pandurra Formation and the Whyalla Sandstone, were also analyzed for comparison. The Pandurra Formation and Whyalla Sandstone samples were obtained from exploration drill holes near OD. The Pandurra Formation samples came from drill holes at the Acropolis (ACD1, ACD15, ACD18), Emmie Bluff (SAE6), Oak Dam (AD1, AD3) and Wirrda Well IOCG prospects (WRD21, WRD31) (Fig. 1B). Samples were taken at intervals throughout the Pandurra Formation to also track any stratigraphic variation in detrital zircon age populations. The Whyalla Sandstone samples were collected from the Emmie Bluff prospect (SAE6) (Fig. 1B). Single spot analyses were recorded on zircon grains. Only those zircon analyses with a discordance of less than 10% were used for population interpretation on probability density plots. The Th/U ratios of zircon analyses were calculated for further comparison of zircon age populations (see supplementary data).

5.1.2. Apatite

Due to the small size of the apatite grains (< 100 μm), U-Pb analyses were conducted *in situ*, on polished mounts, using the same instrument and interpretation software as was used for the analyses of the detrital zircons (see supplement for additional details). The reference apatite OD306 (Thompson et al., 2016) was used as a primary standard. The analyses were further verified using secondary apatite standards 401 (Thompson et al., 2016), Kovdor (Amelin and Zaitsev, 2002) and McClure Mountain (Schoene and Bowring, 2006).

Apatite grains in the sample OD977 (RD2751, 919.6 m) were analyzed. The ablation profiles of the apatite grains are variably heterogeneous; some zones (particularly rims) contain very low U and Pb (Fig. 6B). The ablation profiles of the analyses were split into eight segments (of equal duration) to compensate for the heterogeneity and to improve age calculation statistics (e.g. Davidson et al., 2007; Kamenetsky et al., 2016).

5.2. Results

5.2.1. Zircon

Of the 630 detrital zircon grains analyzed from the quartz-rich sandstone fragments, 289 had a discordance of less than 10%. The detrital zircon age distribution of the quartz-rich sandstone fragments shows three main populations at ca. 2.55–2.35 Ga, ca. 1.7 Ga and ca. 1.59 Ga, and a minor population at ca. 1.85 Ga (Fig. 7A). Identical populations of zircons are present in the red-brown matrix. The similarity in zircon age distribution of the quartz-rich sandstone fragments and enclosing red-brown sandy matrix is consistent with both being derived from brecciation of a single quartz-rich sandstone protolith.

The other bedded clastic facies in the ODBC have a single population of ca. 1.59 Ga detrital zircons (McPhie et al., 2016) (Fig. 7A). Detrital zircon grains in the Pandurra Formation samples from the Acropolis, Emmie Bluff, Oak Dam and Wirrda Well prospects (2416 grains analyzed of which 1024 were < 10% discordant) show the same overall distribution of ages as the quartz-rich sandstone in the ODBC (Fig. 7A); most single samples also have the same overall distribution of zircon ages as the quartz-rich sandstone. The similar age distribution is reflected in the variation in Th/U ratios of the quartz-rich sandstone and Pandurra Formation (see figure in supplementary data). Five of the analyzed samples of Pandurra Formation from drill hole AD3 (Fig. 8) show that the distributions of zircon ages vary uphole: age distributions in lower samples are dominated by a Mesoproterozoic population whereas higher samples have larger Paleoproterozoic and Archean populations (including the appearance of the ca. 1.85 Ga population in the upper samples) (Fig. 8). The Whyalla Sandstone at Emmie Bluff (171 grains analyzed of which 81 were < 10% discordant) has the same zircon age populations identified in the quartz-rich sandstone in the

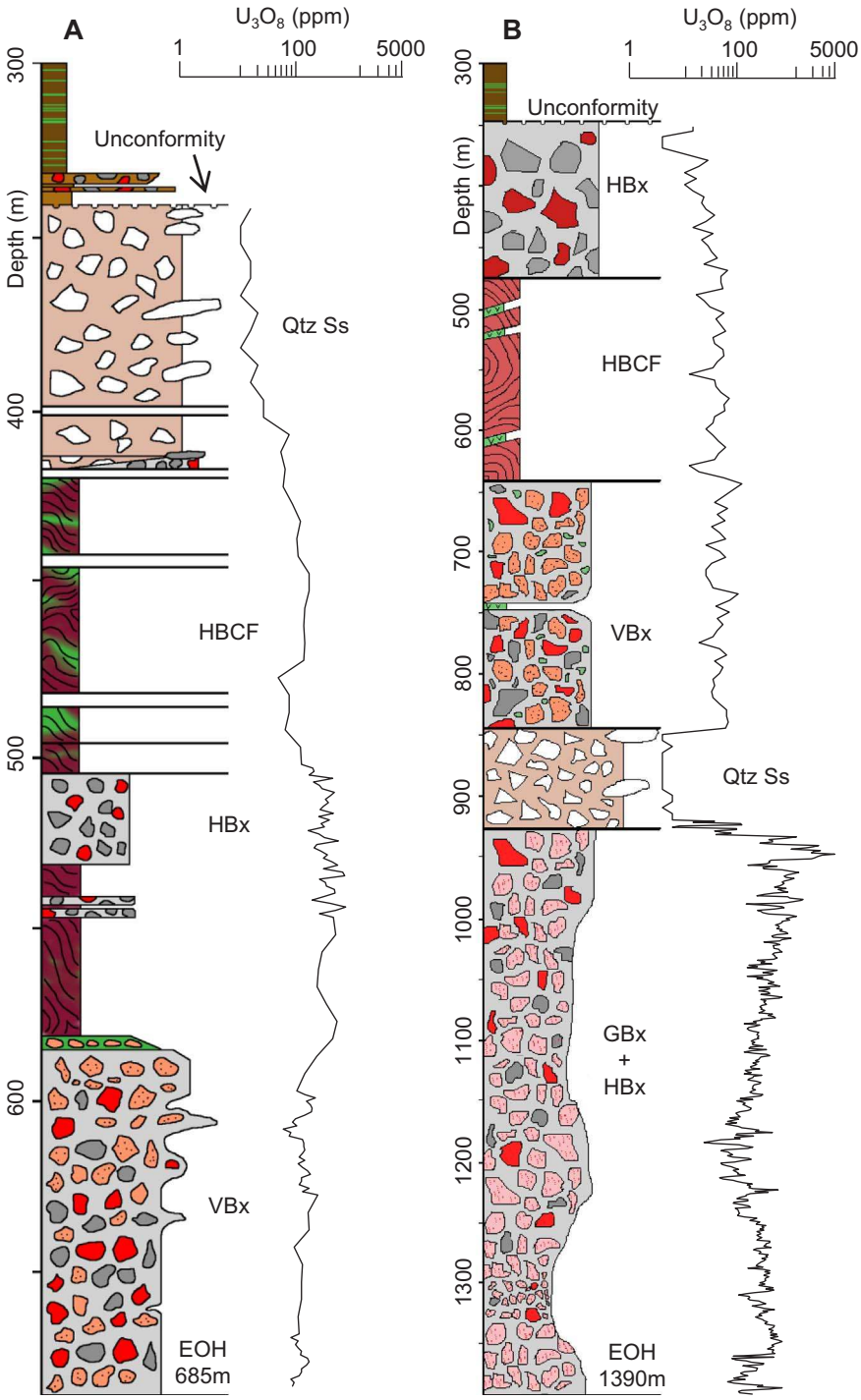


Fig. 4. Lithology logs of drill core A: RD1628 and B: RD2751 and corresponding assay of U_3O_8 grade (detection limit = 4–6 ppm). Note the different vertical scales of the two logs. The interval of quartz-rich sandstone in RD1628 is at ~340–420 m and in RD2751 is at ~840–925 m. The different lithologies and breccia types are juxtaposed by faults (black lines). The trend of U_3O_8 grade reflects that of Cu, Au, Ag and Fe. HBx – Hematite-rich breccia, VBx – Volcanic breccia, GBx – Granite-rich breccia, HBCF – Hematite-rich bedded clastic facies, Qtz Ss – brecciated quartz-rich sandstone.

ODBC, but has additional age populations clustered at ca. 1.2 Ga and ca. 1.1 Ga (Fig. 7A).

5.2.2. Apatite

The most concordant apatite analyses (n = 19) also have the highest U concentrations (100–700 ppm) as well as Th, Ce and total Pb (see supplementary data). The analyses that are more discordant and/or exhibited mixing with common Pb invariably have lower concentrations of U, Th, Ce and Pb. The apatite analyses have been split into multiple ablation segments and presented in a Tera-Wasserburg concordia plot (Fig. 9A, B). The majority of the split analyses cluster near concordia and form a single population which has a $^{207}Pb/^{206}Pb$ age peak at ca. 1.44 Ga (Fig. 7B). The remainder of the split analyses scatter out from the ca. 1.44 Ga population, representing mixing of radiogenic Pb with common Pb as well as analyses with very low $^{238}U/^{206}Pb$ ratios. The majority of the split analyses affected by common Pb and/or with very low $^{238}U/^{206}Pb$ ratios are of grain rims that have low counts of ^{238}U, ^{206}Pb and ^{207}Pb, but relatively constant ^{204}Pb (representing common Pb) (Fig. 6B). The low U and radiogenic Pb counts increase the influence of common Pb on $^{238}U/^{206}Pb$ and $^{207}Pb/^{206}Pb$ ratios. Split analyses containing elevated Fe (> 10,000 ppm) are interpreted to indicate mixing of apatite with fine-grained hematite and have also been excluded from the age interpretation. The final intercept age of the apatite is 1441 ± 15 Ma (MSWD = 3.3, n = 105) (Fig. 9B).

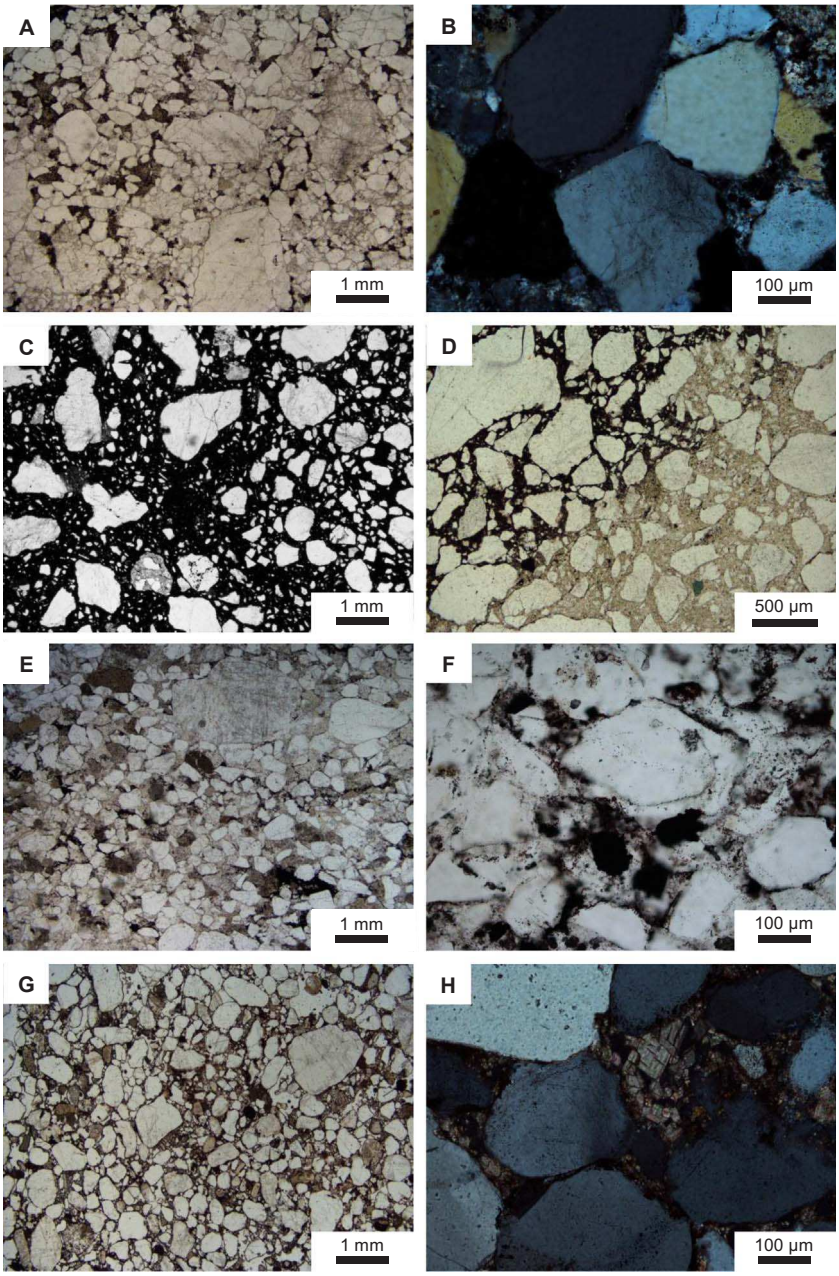


Fig. 5. A-D. Quartz-rich sandstone (Olympic Dam). A: Poorly sorted quartz rich sandstone from a sandstone fragment (crossed polarized transmitted light, RD2751, 900.7 m). B: Syntaxial quartz overgrowths on detrital quartz grains in a sandstone fragment (RD1628, 370 m). C: Red-brown matrix comprising angular, poorly sorted quartz and fine-grained illite/muscovite and hematite cement (RD2751, 855.0 m). D: Part of the red-brown matrix with a hematite-poor halo around a sandstone fragment (off image) (RD1628, 386 m). E, F. Pandurra Formation. E: Poorly sorted quartz-rich sandstone from Pandurra Formation above the Oak Dam prospect (AD3, 548.4 m). F: Syntaxial quartz overgrowths on detrital quartz grains (AD3, 774.1 m). Whyalla Sandstone G: Poorly sorted to bimodal quartz-rich sandstone from Whyalla Sandstone above the Emmie Bluff prospect (SAE6, 376.8 m). H: Carbonate cement between quartz grains in Whyalla Sandstone (SAE6, 376.8 m).

6. Discussion

6.1. Comparison of the quartz-rich sandstone with other bedded clastic facies in the ODBC

The quartz-rich sandstone and the other bedded clastic facies have the same maximum age of deposition of ca. 1.59 Ga, based on the youngest detrital zircon age population. This age reflects the involvement of the Mesoproterozoic Gawler SLIP in the provenance of all the bedded clastic facies. However, the quartz-rich sandstone contains additional zircon populations not present in the other bedded clastic facies, and had a significantly wider provenance that included Archean and Paleoproterozoic successions.

In sections through the bedded clastic facies, the facies associations other than the quartz-rich sandstone occur interbedded with each other and preserved contacts between them are gradational. In RD2751 and RD1628, the brecciated quartz-rich sandstone is separated from other bedded clastic facies by faults or by intervals of hematite-rich or volcanic breccia. Hence, the available data indicate that the quartz-rich sandstone was not originally interbedded with the other bedded clastic facies.

The quartz-rich sandstone is less hydrothermally altered than the other bedded clastic facies, despite juxtaposition with mineralized hematite-rich breccia in the ODBC; hydrothermal minerals are very rare, apart from pervasive, fine-grained hematite in the red-brown breccia matrix. The other bedded clastic facies have been variably affected by texturally destructive hydrothermal alteration (Ehrig et al., 2012) and contain the same hydrothermal mineral assemblage (e.g. hematite, sericite, chlorite, Cu sulfide, siderite, barite, fluorite) as the ore zones in the hematite-rich breccia. McPhie et al. (2016) therefore concluded that the altered and mineralized bedded clastic facies were present at the time of formation of the ODBC and the Cu mineralization event. However, the lower intensity of hydrothermal alteration in the brecciated quartz-rich sandstone suggests it was incorporated into the ODBC separately, at some time after the main mineralization and alteration events (Fig. 5C, D).

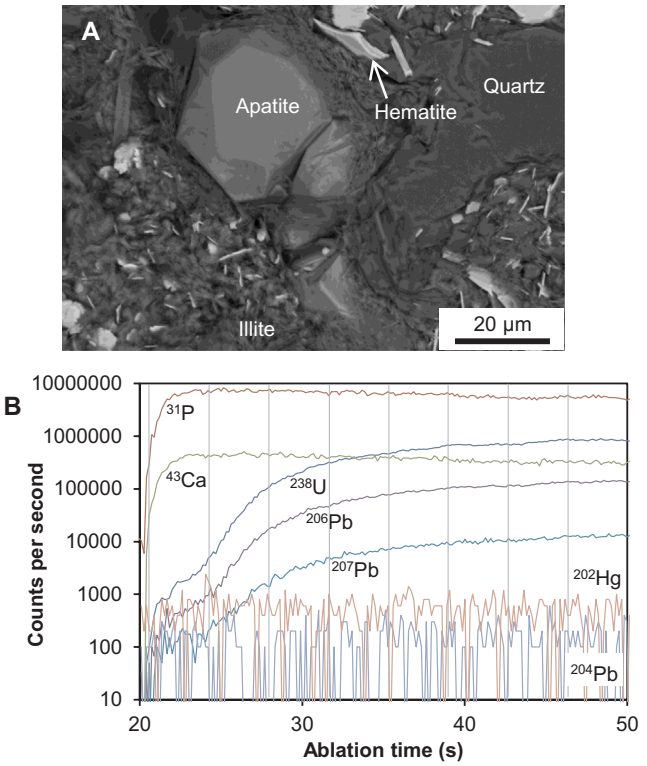


Fig. 6. A: Back-scattered electron image of euhedral apatite interstitial to detrital quartz and intergrown with illite and hematite cement, RD2751, 919.6 m. B: Downhole/time-resolved laser ablation analysis profile of apatite grain showing consistent ^{43}Ca, ^{31}P, ^{202}Hg and ^{204}Pb but low initial ^{238}U and radiogenic Pb. Values are in counts per second. Vertical lines represent the 8 splits of the laser ablation profile; the first three splits produced discordant ages with low apparent $^{238}U/^{206}Pb$ and high $^{207}Pb/^{206}Pb$ ratios.

6.2. Comparison of the quartz-rich sandstone in the ODBC with potential correlates

6.2.1. Pandurra Formation

The Pandurra Formation defines the known extent of the intracontinental Cariewerloo Basin (~42,500 km^2) (Cowley, 1993). The basin has a ~420 km northwesterly extent and is up to ~170 km wide; over 95% of the basin underlies Neoproterozoic and younger sedimentary rocks (Fig. 1). The Pandurra Formation consists of red-bed quartz sandstone that has a maximum thickness of ~1200 m recorded in drill holes from the northern portion of the basin (Keeling et al., 2012). The current margins of the Pandurra Formation in the area around OD have been interpreted to be faults, consistent with the Pandurra Formation having been present above OD originally but subsequently eroded from the top of an uplifted fault block (Cowley, 1993). Reconstructed sections through the Cariewerloo Basin indicate extensive post-depositional displacement of the Pandurra Formation on faults along the eastern basin margin (Cowley, 1993).

The Pandurra Formation sections examined in this study comprise internally massive or graded, well-defined sandstone beds that are commonly cross-stratified. The sandstone is typically poorly sorted and dominated by angular to subrounded fine- to very coarse-grained quartz. The quartz grains are mono- and poly-crystalline, show undulose extinction, and have numerous mineral and fluid inclusions. Syntaxial quartz overgrowths are common. Lithic fragments are variably abundant, comprising up to 50% of some sandstone samples. Minor detrital grains include muscovite, tourmaline, zircon, hematite, rutile and altered ilmenite. The diagenetic assemblage includes ubiquitous hematite coatings, quartz overgrowths and pore-filling dickite and illite cements, all of which have been reported in samples of the Pandurra Formation from other sections (Keeling et al., 2012). Spectral

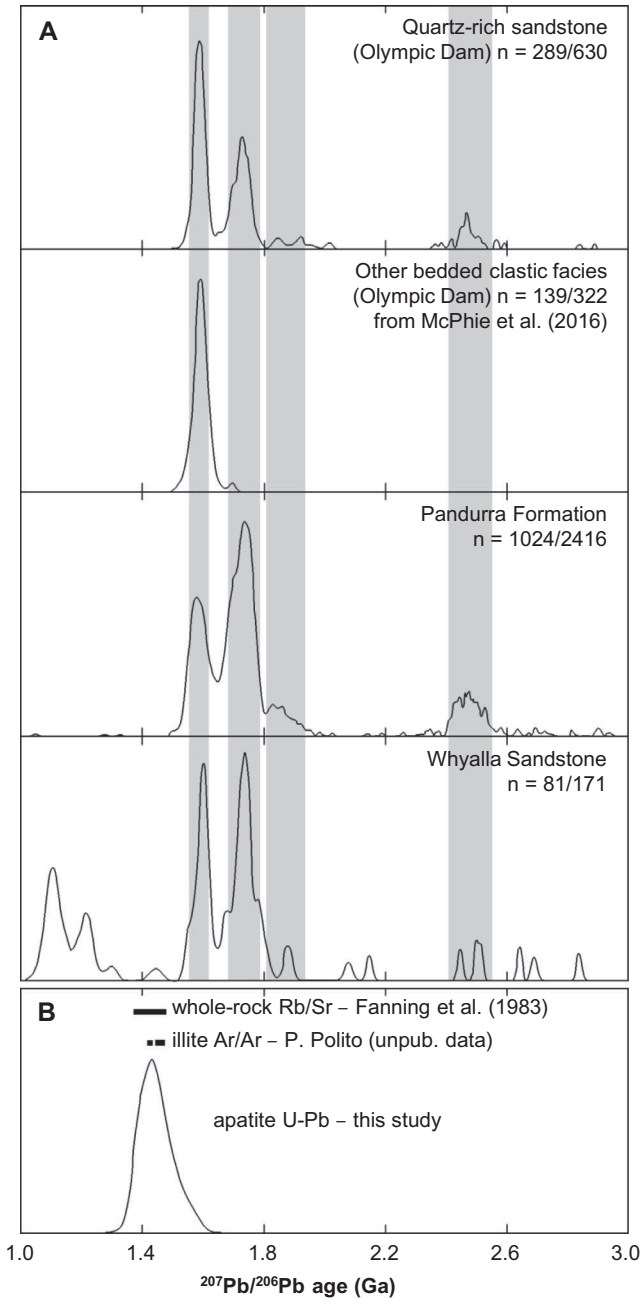


Fig. 7. Probability density distributions of U-Pb age data (< 10% discordant) for A: Detrital zircons from the quartz-rich sandstone and other bedded clastic facies in the ODBC, the Pandurra Formation and Whyalla Sandstone. Gray bars highlight population correlation. Total analyses per sample and proportion of concordant analyses are shown (n). B: Authigenic apatite from the quartz-rich sandstone in OD, prior geochronology of the Pandurra Formation by Fanning et al. (1983) and P. Polito (pers. comm., 2016).

analyses of samples from > 90 drill holes from across the Cariewerloo Basin indicate that only remnant patches of dickite remain; most dickite has been altered to illite/muscovite, due to deep burial and/or circulation of warm, acidic to neutral, saline fluids within the Cariewerloo Basin (Keeling et al., 2015). The detrital mineralogy and diagenetic cement of the Pandurra Formation are very similar to those in the brecciated quartz-rich sandstone in the ODBC (i.e. detrital angular to subrounded, mono- to polycrystalline quartz and lesser lithic fragments, and diagenetic quartz, illite and minor hematite). However, no apatite was observed in the Pandurra Formation samples examined in this study, and apatite has not been reported by other studies of the Pandurra Formation.

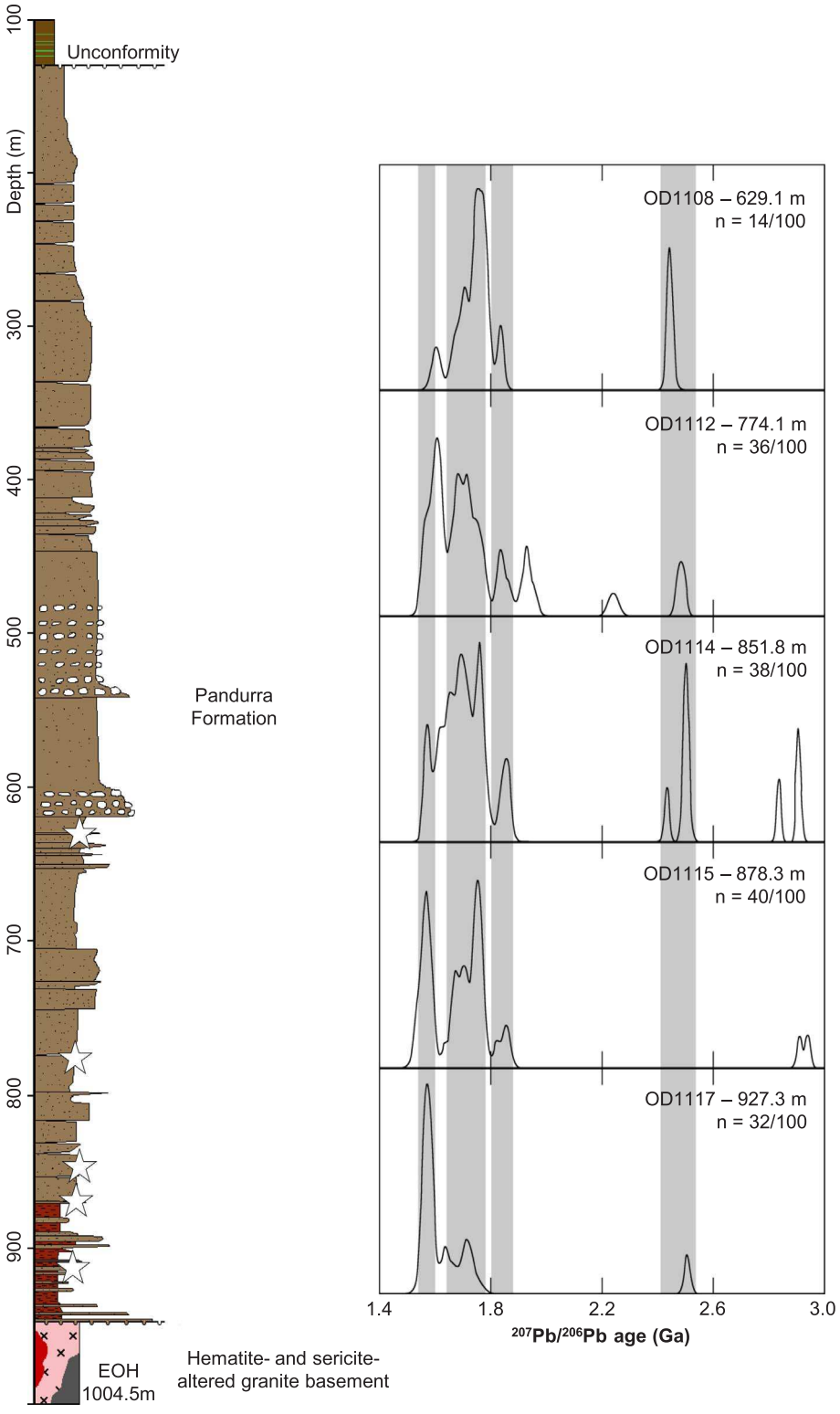


Fig. 8. Log of drill hole AD3 intersecting Pandurra Formation above the Oak Dam IOCG prospect with probability density plots of U-Pb ages (< 10% discordant) of detrital zircons from five samples (depth recorded on plots). Total analyses per sample and proportion of concordant analyses are shown (n). Sample sites are indicated by stars.

The zircon age populations in samples of the Pandurra Formation analyzed in this study are also very similar to those of the quartz-rich sandstone in the ODBC (Fig. 7A), and the similar range of Th/U ratios for each age peak indicates a similar variety of source rocks contributed to both. A similar distribution of zircon ages has been reported for samples of the Pandurra Formation from drill holes farther to the northwest (Peeweena 1 – also known as Red Millers Creek 1) and south (CSR-PY1) (Fanning and Link, 2003) of OD, and from a drill hole to the south (Vanguard-1) (Rollison, 2016) of OD. The detrital zircon populations of drill hole AD3 reveals the appearance (or increasing proportion) of some Paleoproterozoic and Archean age populations in younger Pandurra Formation sandstones (Fig. 8) and suggests the fluvial drainage network was extended or modified over time and/or fluvial erosion exposed older basement beneath areas of thin volcanic cover in the Gawler SLIP (Fig. 8). Rollison (2016) offered a similar interpretation from the Vanguard-1 drill hole. However, the quantity of zircons analyzed in this study limits the reliability of this interpretation (e.g. Andersen, 2005); a more systematic study involving greater

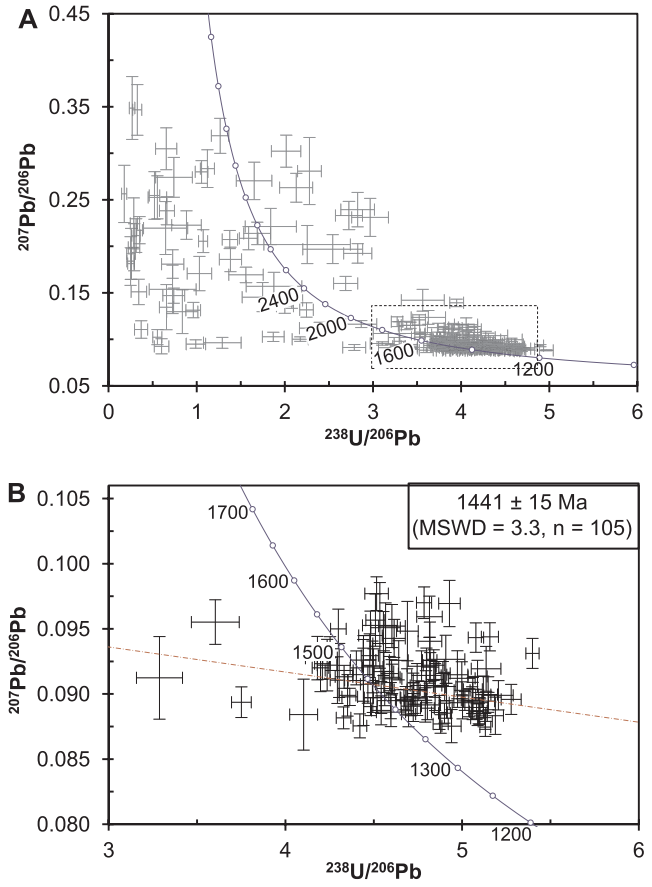


Fig. 9. Authigenic apatite U-Pb geochronology A: Tera-Wasserburg concordia plot showing the fan of split analyses diverging from the ca. 1.44 Ga population due to low U and Pb grains. The box represents the scale of Fig. 9B. B: Tera-Wasserburg concordia plot of the filtered data used for age interpretation with an upper intercept of 1441 ± 15 Ma (MSWD = 3.3, n = 105).

numbers of grains is required to more effectively encapsulate the variation in detrital zircon age populations within and between members of the Pandurra Formation and throughout the Cariewerloo Basin.

The ca. 1.44 Ga age of interstitial authigenic apatite in the brecciated quartz-rich sandstone in the ODBC is interpreted to represent the timing of diagenesis and therefore the minimum depositional age for the quartz-rich sandstone. Authigenic apatite has been described in intracontinental sandstone from the Paleoproterozoic Athabasca and Thelon basins and the Mesoproterozoic Hornby Bay Basin in Canada (Gall and Donaldson, 2006; Davis et al., 2008). The lack of recorded authigenic apatite in the Pandurra Formation and the observation of apatite in only a few fragments of the brecciated quartz-rich sandstone in the ODBC suggest apatite is a relatively rare phase in the Cariewerloo Basin. A whole rock Rb/Sr age of 1424 ± 51 Ma for Pandurra Formation siltstone beds in drill hole Peeweena 1 drilled in the northern Cariewerloo Basin, was interpreted as the minimum age of deposition (Fanning et al., 1983). This age is supported by unpublished authigenic illite/muscovite ages of 1426 ± 6 and 1458 ± 11 Ma ($^{40}Ar/^{39}Ar$; P. Polito, 2016, pers. comm.) for samples of basal Pandurra Formation in drill hole HHD1 (1071.6 m and 1046.0 m down hole, respectively), located ~40 km southwest of OD. Our result of ca. 1.44 Ga for the crystallization of euhedral, authigenic apatite in the quartz-rich sandstone cement is consistent with available data on the timing of deposition or early diagenesis/lithification of the Pandurra Formation (Fig. 7B). Coupled with the consistent detrital zircon age populations and mineralogy, the Pandurra Formation correlates very strongly with the brecciated quartz-rich sandstone in the ODBC.

6.2.2. Whyalla sandstone

Another possible protolith for the brecciated quartz-rich sandstone in the ODBC is the Neoproterozoic Whyalla Sandstone. The Whyalla Sandstone extends ~25,000 km^2 across the Stuart Shelf; it has a ~470 km north to northwest extent and is up to ~170 km east to west (Fig. 1). This Neoproterozoic sandstone at one time may have extended across the ODBC and been removed later by erosion, as it is not preserved directly over the ODBC. The sandstone is predominantly medium to very coarse-grained, and composed of well-rounded quartz grains that are typically bimodal (Fig. 5G) (Williams, 1998). Whyalla Sandstone from drill hole SAE6 has a similar mineralogy to the quartz-rich sandstone in the ODBC, however, the bimodal grain size distribution, rounded grains and carbonate-dominated cement in the Whyalla Sandstone (Fig. 5G, H) are not characteristics of the quartz-rich sandstone. Also, the Whyalla Sandstone (Fig. 7A) contains 1.2–1.1 Ga zircons which are not present in the brecciated quartz-rich sandstone at OD.

6.2.3. Sedimentary successions related to the GRV

The GRV was present above the RDG at OD prior to formation of the ODBC (McPhie et al., 2011; Ehrig et al., 2012). Regionally, sedimentary facies are very minor in the GRV (Blissett et al., 1993; Allen et al., 2008) though locally, they may be significant, for example, at Prominent Hill (Bull et al., 2015) and at Roopena (Fresh Well Formation; McAvaney and Wade, 2015). These successions comprise sandstone and conglomerate intercalated with GRV volcanic units, have sedimentary inputs from pre-Gawler SLIP lithologies and some contain zircons older than 1.59 Ga (e.g. Fresh Well Formation; Johnson, 1993). However, they are dominated by volcanic and metamorphic lithic clasts, distinct from the quartz-dominated mineralogy of the quartz-rich sandstone in the ODBC.

6.3. Probable protolith of the quartz-rich sandstone

We conclude that the brecciated quartz-rich sandstone in the ODBC is most probably part of the Pandurra Formation. In particular, the components and bedforms are identical to those in quartz sandstone of the Pandurra Formation; the timing of diagenesis determined for authigenic apatite in the cement of the sandstone fragments is consistent with the timeframe for deposition and diagenesis of the Pandurra Formation; the populations of detrital zircons match those in the Pandurra Formation and clearly distinguish the quartz-rich sandstone from other bedded clastic facies in the ODBC; and the detrital and cement mineralogy are closely comparable with those of quartz sandstone in the Pandurra Formation.

Given that we have found remnants of the Pandurra Formation (ca. 1.44 Ga) within the ODBC (largely ca. 1.59 Ga), and that those remnants are relatively unaltered, the Cariewerloo Basin at one time must have covered the deposit and remained in place long enough for the Pandurra Formation to become lithified (i.e. after the diagenetic changes at ca. 1.44 Ga). If this conclusion is correct, then the Pandurra Formation was subsequently eroded from the uplifted fault block containing the ODBC, prior to deposition of the Nuccaleena Formation (ca. 635 Ma; Rose and Maloof, 2010), the oldest of the Neoproterozoic units directly overlying the ODBC (Roberts and Hudson, 1983). The complete erosion of the Pandurra Formation from above the ODBC implies that an unknown volume of the ODBC was also eroded at the same time.

6.4. Incorporation of the Pandurra Formation into the ODBC

The brecciated fragments of probable Pandurra Formation occur just below the unconformity surface at the top of the ODBC (RD1628), and over 400 m (RD2751) below the unconformity in faulted contact with hematite-rich breccia and bedded clastic facies. Tectonic activity is the most likely mechanism for incorporation of Pandurra Formation into the ODBC. The ODBC includes subvertical northwest-striking faults

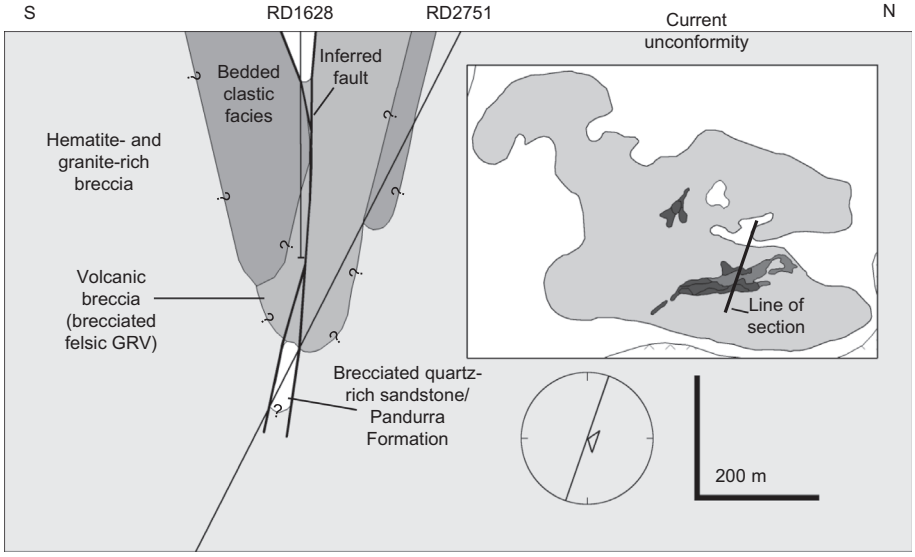


Fig. 10. Cross-section of the ODBC showing the position of the incorporated remnants of the Pandurra Formation (brecciated quartz-rich sandstone) recorded in drill holes RD1628 and RD2751. Boundaries of lithologies (bedded clastic facies, volcanic breccia, brecciated quartz-rich sandstone) have been approximated with reference to Ehrig et al. (2012), McPhie et al. (2016) and unpublished reports by K. Orth. An inferred fault that may have been involved in incorporation of the Pandurra Formation remnants is shown. Inset shows the position of the cross-section relative to the breccia complex.

and northeast- to eastnortheast-striking faults that dip steeply northwest (Hayward and Skirrow, 2010; Ehrig et al., 2012). The brecciated Pandurra Formation within the ODBC is near the Jubilee Fault Zone (JFZ, also referred to locally as Masher's Fault) (Figs. 2, 10). The JFZ is a major subvertical, crustal-scale structure that has evidence of reactivation since the Neoproterozoic; other adjacent fault sets and splays in the ODBC also show evidence of localized reactivation (Hayward and Skirrow, 2010; Ehrig et al., 2012). It is noted that the majority of the preserved southern, steeply dipping portion of the bedded clastic facies are adjacent to the JFZ (Figs. 2, 10).

The position of the Pandurra Formation remnants and other bedded clastic facies adjacent to the JFZ suggests this fault zone and/or adjacent faults were involved in the incorporation of these lithologies into the ODBC. The southern preserved portion of the bedded clastic facies has an elongate, steeply-dipping geometry (McPhie et al., 2016). The two drill core intersections of the Pandurra Formation hint at a subvertical geometry (and may be connected, Fig. 10), potentially occupying a single fault. The thorough brecciation of the Pandurra Formation remnants and weak hydrothermal alteration relative to the other bedded clastic facies imply the Pandurra Formation was incorporated separately from the other bedded clastic facies (Fig. 10). As the other bedded clastic facies are inferred to have been present at the time of formation of the ODBC (McPhie et al., 2016), they were probably incorporated prior to the deposition of the ca. 1.44 Ga Pandurra Formation.

Incorporation of fragments of Pandurra Formation may have involved propagation of the JFZ, and associated reactivated faults, upwards into the overlying sandstone, causing brecciation and local entrainment of slices or fragments of sandstone along those faults. The faults bounding the remnants of Pandurra Formation lack dateable minerals and therefore the timing of tectonic movement leading to the entrainment of the sandstone fragments cannot be determined. As a result, constraints on the timing of incorporation are limited to maximum and minimum ages. The preservation of large fragments of the Pandurra Formation indicates incorporation occurred after lithification (inferred to be ca. 1.44 Ga), providing a maximum age. The late Neoproterozoic Stuart Shelf formations above the unconformity have not been faulted or otherwise incorporated into the ODBC, giving a minimum age of incorporation of ca. 635 Ma (e.g. Nuccaleena Formation; Rose and Maloof, 2010). The late Neoproterozoic Stuart Shelf formations also provide a minimum age for erosion of the Pandurra Formation from the top of the ODBC. Post-1.44 Ga faults in the vicinity of OD define much of the eastern margin of the Pandurra Formation but do not affect the distribution of the overlying Stuart Shelf sedimentary formations (Cowley, 1993); the timing of movements on these faults, however, is presently unknown.

The Musgrave Orogeny (ca. 1.2 Ga; Major and Conor, 1993) and the Gairdner Dyke Swarm event (0.83 Ga; Wingate et al., 1998) are tectonic episodes that affected the Gawler Craton within the timeframe envisaged for incorporation of Pandurra Formation into the ODBC. The Musgrave Orogeny was centered on the Musgrave Province over 600 km away, but there is increasing evidence for an associated thermal pulse throughout much of the Gawler Craton (e.g. Reid et al., 2017), including fluid circulation in the Cariewerloo Basin (Keeling et al., 2015). However, no tectonic activity in the Gawler Craton has been correlated specifically with the Musgrave Orogeny. The intrusion of the Gairdner Dyke Swarm was associated with significant extension (Wingate et al., 1998), including at OD (Huang et al., 2015). A spatial association between Gairdner dolerite dykes and the Pandurra Formation remnants in the ODBC would be expected if the extension associated with the dykes was responsible for incorporation of the Pandurra Formation. A probable Gairdner dolerite dyke is present 200 m uphole of the interval of brecciated Pandurra Formation in RD2751; however, there are no dykes in contact with the intervals of brecciated Pandurra Formation.

The Pandurra Formation may have been incorporated in much greater volumes than currently observed, the remnants having potentially been obliterated by brecciation and hematite alteration. Quartz is the only protolith relic in the most hematite-altered breccia zones. A search for pre-1.59 Ga zircons in the intensely altered hematite-rich breccia could reveal the presence of additional Pandurra Formation quartz-rich sandstone protolith.

6.5. *Implications for modification of the U resource at Olympic Dam*

Textural relationships among the copper sulfides and the uranium minerals, and geological constraints on the timing of precipitation of the copper sulfides have previously been interpreted to indicate that these minerals co-precipitated at ca. 1.59 Ga (Reeve et al., 1990; Johnson and Cross, 1995), even though the first attempt to date the U minerals gave younger ages (Trueman, 1986). Although there is now evidence of U having been present in OD at ca. 1.59 Ga (Ciobanu et al., 2013; Apukhtina et al., accepted), continuing studies of U minerals in the ODBC support the early results of Trueman (1986) and indicate the U resource has continued to be modified after ca 1.59 Ga (Kirchenbaur et al., 2016; Macmillan et al., 2016). The earliest identified uraninite generation in the ODBC has REE signatures consistent with derivation from a high-temperature magmatic fluid whereas the signatures of later

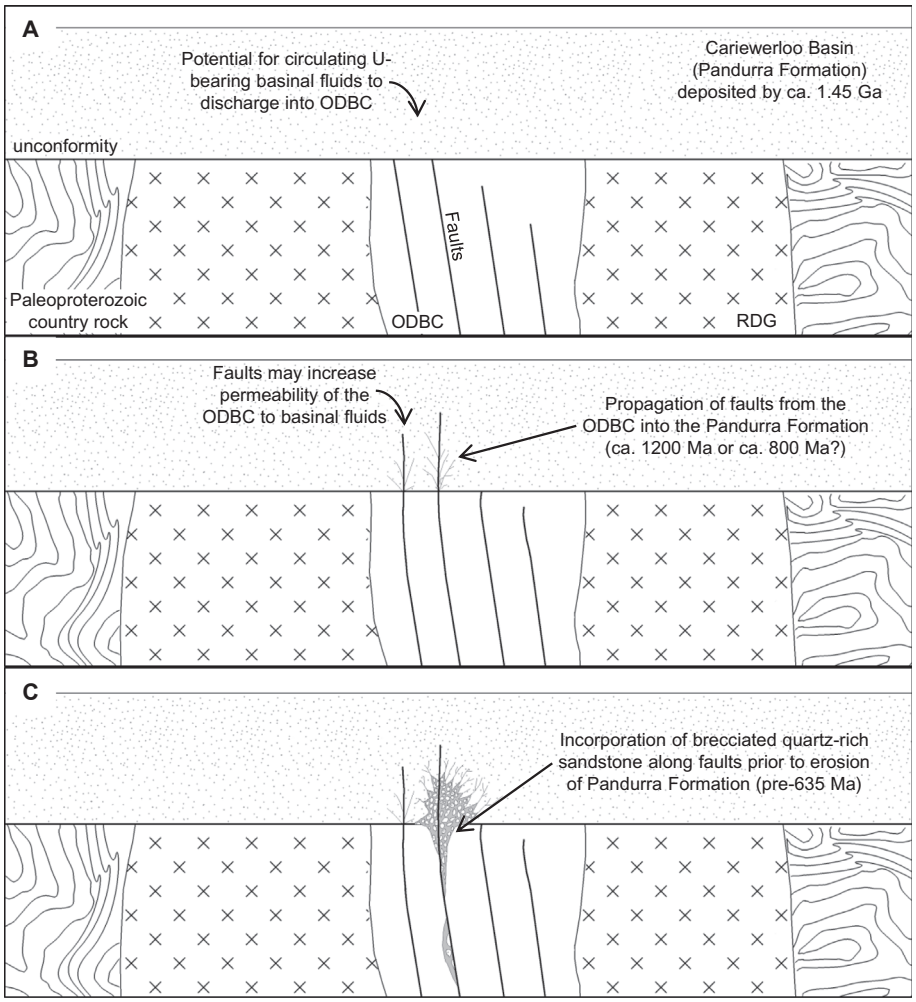


Fig. 11. A: Schematic reconstruction of the Cariewerloo Basin overlying the ODBC and RDG. B: Propagation of faults from the ODBC into the Pandurra Formation may have facilitated discharge of circulating basinal fluids into the ODBC. C: Movement along these faults may have entrained fragments of quartz-rich sandstone into the ODBC from the overlying Pandurra Formation prior to its erosion.

generations are more consistent with precipitation from low-T (< 250 °C) fluids (Mercadier et al., 2011; Macmillan et al., 2016). Post-1.59 Ga ages of uraninite have generally been attributed to remobilization and reprecipitation of U minerals (Reeve et al., 1990; Johnson and Cross, 1995). Similarly, the deposit-wide deficit in Pb relative to the amount of U with an entirely ca. 1.59 Ga age (Trueman, 1986) has been attributed to episodic Pb loss from the deposit (Reeve et al., 1990). However, the Pb deficit only exists if the entire U resource is ca. 1.59 Ga in age and is also consistent with post-1.59 Ga addition of U to the deposit.

The Cariewerloo Basin is a potential source and conduit for post-1.59 Ga U, given that the Pandurra Formation is now known to have unconformably overlain the ODBC. The thick continental sandstone of the Pandurra Formation contained circulating oxygenated, saline, acidic fluids (Keeling et al., 2012). In addition to fluid movement associated with diagenesis at ca. 1.4 Ga, extensive fluid circulation in the Cariewerloo Basin at ca. 1.2 Ga and ca. 0.5 Ga has been inferred from the distribution and timing of crystallization of illite cements (Keeling et al., 2015). Such basin-derived fluids are widely implicated in the formation of unconformity-related U deposits associated with Proterozoic continental basins (Derome et al., 2005; Richard et al., 2012). The fluids are capable of liberating U from accessory U-bearing phases (e.g. volcanic glass, zircon, monazite, uranothorite) either in the basin succession or the underlying basement rocks (Kyser and Cuney, 2008). The source rocks and basement of the Pandurra Formation include lithologies with anomalous levels of U (e.g. Hiltaba Suite, and GRV to a lesser extent) (Neumann et al., 2000; Agangi et al., 2010). Hence, U sources (detrital grains or underlying basement) would have been available to the fluids circulating in the Cariewerloo Basin.

The geological setting, source rocks and interpreted fluid chemistry of the Cariewerloo Basin meet the requirements for mobilization of U by basin fluids (e.g. Kyser and Cuney, 2008). The faults that ruptured and re-located the Pandurra Formation from its original position above the ODBC could have also provided a pathway for fluids circulating within the Cariewerloo Basin into the ODBC (Fig. 11). These fluids may have upgraded or downgraded the deposit through precipitation or leaching of U minerals, respectively.

Unconformity-related U deposits are associated with unconformities that juxtapose reducing basement rocks with oxidized fluids in overlying sedimentary basins (Kyser and Cuney, 2008). Reduction of mobile U^{6+} by Fe^{2+} is considered to be a plausible mechanism for the formation of unconformity-related U deposits (Yeo and Potter, 2010). Within the ODBC, siderite and magnetite are preserved mainly on the deposit margins and at depth (Ehrig et al., 2012). Both minerals are a potential source of Fe^{2+} ions capable of reducing U^{6+} to immobile U^{4+} and were likely more abundant throughout the ODBC (Reeve et al., 1990). Magnetite can transform to hematite in the presence of acidic fluids, releasing Fe^{2+} in the process (Otake et al., 2007) but Fe^{2+} in magnetite is also capable of directly reducing U^{6+} (Scott et al., 2005). Siderite has been experimentally shown to be capable of reducing U^{6+} to U^{4+} in neutral and basic conditions (Ithurbide et al., 2010) but no data exist for acidic conditions.

7. Conclusions

We conclude that the brecciated quartz-rich sandstone in the ODBC

is most probably part of the Pandurra Formation due to the positive comparison of texture, bedforms, detrital and cement mineralogy, detrital zircon age populations and diagenetic age. The presence of the Pandurra Formation within the ODBC requires that the Cariewerloo Basin at one time extended over the ODBC and that tectonic activity occurred on a scale large enough to brecciate and entrain the sandstone after ca. 1.44 Ga and before the Pandurra Formation was eroded from above OD. The potential for generation and circulation of oxidized, acidic fluids in the Cariewerloo Basin, capable of mobilizing U, raises the possibility that such fluids contributed to the development or modification of the world's largest U deposit. Addition of U from the Cariewerloo Basin is consistent with emerging evidence of post-1.59 Ga modification of the U resource in OD.

Acknowledgements

This paper represents part of the PhD project undertaken by A.R. Cherry while supported by an Australian Postgraduate Award scholarship. This project was funded by the Australian Research Council and BHP Billiton Olympic Dam with additional support from a student research grant awarded by the Society of Economic Geologists Foundation. Discussions with K. Cross, N. Chapman and M. Ferguson are gratefully acknowledged. This manuscript was greatly improved by the constructive comments of an anonymous reviewer. Geochronology and SWIR analyses were obtained with the help of J. Thompson and C. Harraden, respectively.

Appendix A. Supplementary data

Supplementary data associated with this article can be found, in the online version, at http://dx.doi.org/10.1016/j.precamres.2017.08.002.

References

Agangi, A., Kamenetsky, V.S., McPhie, J., 2010. The role of fluorine in the concentration and transport of lithophile trace elements in felsic magmas: insights from the Gawler Range Volcanics, South Australia. Chem. Geol. 273, 314–325.

Allen, S.R., McPhie, J., Ferris, G., Simpson, C., 2008. Evolution and architecture of a large felsic Igneous Province in western Laurentia: the 1.6 Ga Gawler Range Volcanics, South Australia. J. Volcanol. Geothermal Res. 172, 132–147.

Amelin, Y., Zaitsev, A.N., 2002. Precise geochronology of phoscorites and carbonatites: the critical role of U-series disequilibrium in age interpretations. Geochim. Cosmochim. Acta 66, 2399–2419.

Andersen, T., 2005. Detrital zircons as tracers of sedimentary provenance: limiting conditions from statistics and numerical simulation. Chem. Geol. 216, 249–270.

Apukhtina, O.A., Kamenetsky, V.S., Ehrig, K., Kamenetsky, M.B., Maas, R., Thompson, J., McPhie, J., Ciobanu, C.L., Cook, N.J., accepted, Deep, early mineralization at the Olympic Dam Cu-U-Au-Ag deposit, South Australia, Econ. Geol., p. 24.

BHP Billiton, 2016, Annual Report 2016.

Black, L.P., Gulson, B.L., 1978. The age of the Mud Tank Carbonatite, Strangways Range, Northern Territory. BMR J. Aust. Geol. Geophys. 3, 227–232.

Black, L.P., Kamo, S.L., Allen, C.M., Aleinikoff, J.N., Davis, D.W., Korsch, R.J., Foudoulis, C., 2003. TEMORA 1: a new zircon standard for Phanerozoic U-Pb geochronology. Chem. Geol. 200, 155–170.

Blissett, A.H., Creaser, R.A., Daly, S.J., Flint, R.B., Parker, A.J., 1993, Gawler Range Volcanics. In: Drexel, J.F., Preiss, W.V., Parker A.J., (Eds.), The Geology of South Australia. Vol. 1, The Precambrian, Volume Bulletin 54: Geological Survey of South Australia, p. 107–131.

Bull, S., Meffre, S., Allen, M., Freeman, H., Tomkinson, M., Williams, P., Volcanosedimentary and chronostratigraphic architecture of the host rock succession at Prominent Hill, South Australia. In: Proceedings SEG 2015: World-Class Ore Deposits: Discovery to Recovery, Hobart, Tasmania, Australia, September 27–30, 2015 2015, Society of Economic Geologists, p. 1.

Ciobanu, C.L., Wade, B.P., Cook, N.J., Mumm, A.S., Giles, D., 2013. Uranium-bearing hematite from the Olympic Dam Cu-U-Au deposit, South Australia: a geochemical tracer and reconnaissance Pb-Pb geochronometer. Precambrian Res. 238, 129–147.

Clark, J., Poznik, N., Ehrig, K., 2016, Unravelling the giant: evidence for post-mineralisation modification of the Olympic Dam Cu-Au-U-Ag deposit, Gawler Craton, South Australia, Australian Earth Sciences Convention, Volume 118: Adelaide, Australia, Geological Society of Australia Abstracts, p. 494.

Cowley, W.M., 1993, Pandurra Formation. In: Drexel, J.F., Preiss, W.V., Park, J.K., (Eds.), The Geology of South Australia. vol. 1, The Precambrian: Geological Survey of South Australia, pp. 139–142.

Davidson, G.J., Paterson, H., Meffre, S., Berry, R.F., 2007. Characteristics and origin of the Oak Dam East breccia-hosted, iron oxide Cu-U-(Au) deposit: Olympic Dam region, Gawler craton, South Australia. Econ. Geol. 102, 1471–1498.

Davis, W.J., Rainbird, R.R., Gall, Q., Jefferson, C.J., 2008. In situ U-Pb dating of diagenetic apatite and xenotime: Paleofluid flow history within the Thelon, Athabasca and Hornby Bay basins. Geochim. Cosmochim. Acta 72, A203.

Derome, D., Cathelineau, M., Cuney, M., Fabre, C., Lhomme, T., Banks, D.A., 2005. Mixing of sodic and calcic brines and uranium deposition at McArthur River, Saskatchewan, Canada: a Raman and laser-induced breakdown spectroscopic study of fluid inclusions. Econ. Geol. 100, 1529–1545.

Drexel, J.F., Preiss, W.V., Parker, A.J., 1993, The Geology of South Australia, Volume 1, The Precambrian: Geological Survey of South Australia, Bulletin, vol. 54, p. 242p.

Ehrig, K., McPhie, J., Kamenetsky, V.S., 2012, Geology and mineralogical zonation of the Olympic Dam Iron Oxide Cu-U-Au-Ag Deposit, South Australia. In: Hedenquist, J.W., Harris, M., Camus, F., (Eds.), Economic Geology Special Publication 16, pp. 237–267.

Fanning, C.M., Flint, R.B., Preiss, W.V., 1983, Geochronology of the Pandurra Formation: Geological Survey of South Australia Quarterly Geological Notes, vol. 88, pp. 11–16.

Fanning, C.M., Link, P.K., 2003, Detrital zircon provenance of the Mesoproterozoic Pandurra Formation, South Australia: Gawler Craton – zircon population and implications for the Belt Supergroup, Abstracts with Programs, Volume 35: Seattle, Geological Society of America, p. 465.

Gall, Q., Donaldson, J.A., 2006. Diagenetic fluorapatite and aluminium phosphate-sulphate in the Paleoproterozoic Thelon Formation and Hornby Bay Group, northwestern Canadian Shield. Can. J. Earth Sci. 43, 617–629.

Hand, M., Reid, A., Jagodzinski, L., 2007. Tectonic framework and evolution of the Gawler Craton, southern Australia. Econ. Geol. 102, 1377–1395.

Hayward, N., Skirrow, R., 2010, Geodynamic setting and controls on iron oxide Cu-Au (± U) ore in the Gawler Craton, South Australia: hydrothermal iron oxide copper-gold and related deposits: a global perspective, vol. 3, pp. 105–131.

Hitzman, M.W., Oreskes, N., Einaudi, M.T., 1992. Geological characteristics and tectonic setting of Proterozoic Iron-Oxide (Cu-U-Au-REE) Deposits. Precambr. Res. 58, 241–287.

Hitzman, M.W., Valenta, R.K., 2005. Uranium in iron oxide-copper-gold (IOCG) systems. Econ. Geol. 100, 1657–1661.

Huang, Q., Kamenetsky, V.S., McPhie, J., Ehrig, K., Meffre, S., Maas, R., Thompson, J., Kamenetsky, M., Chambefort, I., Apukhtina, O., Hu, Y., 2015. Neoproterozoic (ca. 820–830 Ma) mafic dykes at Olympic Dam, South Australia: links with the Gairdner Large Igneous Province. Precambrian Res. 271, 160–172.

Ithurbide, A., Peulon, S., Miserque, F., Beaucaire, C., Chausse, A., 2010. Retention and redox behaviour of uranium(VI) by siderite ($FeCO_3$). Radiochim. Acta 98, 563–568.

Jackson, S.E., Pearson, N.J., Griffin, W.L., Belousova, E.A., 2004. The application of laser ablation-inductively coupled plasma-mass spectrometry to in situ U-Pb zircon geochronology. Chem. Geol. 211, 47–69.

Jagodzinski, E.A., 2014, The age of magmatic and hydrothermal zircon at Olympic Dam, Australian Earth Sciences Convention, Volume 110: Newcastle, Australia, Geological Society of Australia Abstracts, p. 260.

Jagodzinski, E.A., Reid, A., Crowley, J., McAvaney, S.O., Wade, C., 2016, Precise zircon U-Pb dating of a Mesoproterozoic silicic large igneous province: the Gawler Range Volcanics and Benageric Volcanic Suite, South Australia, Australian Earth Sciences Convention, Volume 118: Adelaide, Australia, Geological Society of Australia, p. 494.

Johnson, J.P., 1993. The geochronology and radiogenic isotope systematics of the Olympic Dam copper-uranium-gold-silver deposit, South Australia [Ph.D. thesis], The Australian National University, 318 p.

Johnson, J.P., Cross, K.C., 1995. U-Pb geochronological constraints on the genesis of the Olympic Dam Cu-U-Au-Ag deposit, South Australia. Econ. Geol. 90, 1046–1063.

Kamenetsky, V.S., Lygin, A.V., Foster, J.G., Meffre, S., Maas, R., Kamenetsky, M.B., Goemann, K., Beresford, S.W., 2016. A story of olivine from the McIvor Hill complex (Tasmania, Australia): clues to the origin of the Avebury metasomatic Ni sulfide deposit. Am. Mineral. 101, 1321–1331.

Keeling, J.L., Mauger, A.J., Wilson, T., Raven, M.D., 2012, Diagenetic clay mineral distribution in Mesoproterozoic sandstones of the Cariewerloo Basin, South Australia – implications for uranium mobilisation, in Proceedings Australian Regolith Geoscientists Association and Australian Clay Minerals Society Conference, Mildura, Victoria, 7–9 February 2012, pp. 17–21.

Keeling, J.L., Wilson, T., Mauger, A., 2015, Gawler Craton: potential for unconformity-related uranium – spectral insights: South Australian Resources & Energy Investment Conference Abstracts, Department of State Development, South Australia, Report Book 2015/00006, pp. 35–37.

Kirchenbaur, M., Maas, R., Ehrig, K., Kamenetsky, V.S., Strub, E., Ballhaus, C., Munker, C., 2016. Uranium and Sm isotope studies of the supergiant Olympic Dam Cu-Au-U-Ag deposit, South Australia. Geochim. Cosmochim. Acta 180, 15–32.

Kyser, K., Cuney, M., 2008. Chapter 8: Unconformity-related uranium deposits. In: Cuney, M., Kyser, K., (Eds.), Recent and not-so-recent developments in uranium deposits and implications for exploration, Volume 39: Quebec City, Mineralogical Association of Canada Short Course Series.

Li, X.H., Tang, G.Q., Gong, B., Yang, Y.H., Hou, K.J., Hu, Z.C., Li, Q.L., Liu, Y., Li, W.X., 2013. Qinghu zircon: a working reference for microbeam analysis of U-Pb age and Hf and O isotopes. Chin. Sci. Bull. 58, 4647–4654.

Ludwig, K.R., 2008, User's manual for Isoplot 3.70: a geochronological toolkit for Microsoft Excel: Berkeley Geochronological Center Special Publication, v. 4.

Macmillan, E., Cook, N.J., Ehrig, K., Ciobanu, C.L., Pring, A., 2016. Uraninite from the Olympic Dam IOCG-U-Ag deposit: linking textural and compositional variation to temporal evolution. Am. Mineral. 101, 1295–1320.

Major, R.B., Conor, C.H.H., 1993. Musgrave Block. In: Drexel, J.F., Preiss, W.V., A.J., P., (Eds.), The geology of South Australia. Vol. 1, The Precambrian: South Australia, Geological Survey of South Australia, pp. 156–167.

McAvaney, S.O., Wade, C.E., 2015, Stratigraphy of the Lower Gawler Range Volcanics in the Roopena area, northeastern Eyre Peninsula: Department of State Development.

McPhie, J., Kamenetsky, V.S., Chambefort, I., Ehrig, K., Green, N., 2011. Origin of the supergiant Olympic Dam Cu-U-Au-Ag deposit, South Australia: was a sedimentary basin involved? Geology 39, 795–798.
McPhie, J., Orth, K., Kamenetsky, V., Kamenetsky, M., Ehrig, K., 2016. Characteristics, origin and significance of Mesoproterozoic bedded clastic facies at the Olympic Dam Cu-U-Au-Ag deposit, South Australia. Precambrian Res. 276, 85–100.
Mercadier, J., Cuney, M., Lach, P., Boiron, M.-C., Bonhoure, J., Richard, A., Liesen, M., Kister, P., 2011. Origin of uranium deposits revealed by their rare earth element signature. Terra Nova 23, 264–269.
Neumann, N., Sandiford, M., Foden, J., 2000. Regional geochemistry and continental heat flow: implications for the origin of the South Australian heat flow anomaly. Earth Planet. Sci. Lett. 183, 107–120.
Oreskes, N., Einaudi, M.T., 1990. Origin of rare-earth element-enriched hematite breccias at the Olympic-Dam Cu-U-Au-Ag Deposit, Roxby Downs, South Australia. Econ. Geol. 85, 1–28.
Otake, T., Wesolowski, D.J., Anovitz, L.M., Allard, L.F., Ohmoto, H., 2007. Experimental evidence for non-redox transformations between magnetite and hematite under H2-rich hydrothermal conditions. Earth Planet. Sci. Lett. 257, 60–70.
Preiss, W.V., 1987. The Adelaide Geosyncline. Late Proterozoic stratigraphy, sedimentation, palaeontology and tectonics. Geological Survey of South Australia, Bulletin 53, 438.
Preiss, 1993. Neoproterozoic. In: Drexel, J.F., Preiss, W.V., A.J., P., (Eds.), The geology of South Australia, Volume 1, the Precambrian, Volume 54: South Australia, Geological Survey of South Australia Bulletin, pp. 170–203.
Reeve, J.S., Cross, K.C., Smith, R.N., Oreskes, N., 1990. Olympic Dam copper-uranium-gold-silver deposit. In: Hughes, F.E., (Ed.), Geology of the mineral deposits of Australia and Papua New Guinea, Australasian Institute of Mining and Metallurgy, Melbourne, Monograph 14, pp. 1009–1035.
Reid, A.J., Jourdan, F., Jagodzinski, E., 2017. Mesoproterozoic fluid events affect Archean crust in the northern Olympic Cu-Au Province, Gawler Craton: insights from 40Ar/39Ar thermochronology. Aust. J. Earth Sci. 1–17.
Richard, A., Rozsypal, C., Mercadier, J., Banks, D.A., Cuney, M., Boiron, M.-C., Cathelineau, M., 2012. Giant uranium deposits formed from exceptionally uranium-rich acidic brines. Nat. Geosci. 5, 142–146.
Roberts, D.E., Hudson, G.R.T., 1983. The Olympic Dam copper-uranium-gold deposit, Roxby Downs, South Australia. Econ. Geol. 78, 799–822.
Rollison, L., 2016, Stratigraphy, sedimentology and geochemistry of the Pandurra Formation [PhD Thesis], University of Adelaide, 157 p.
Rose, C.V., Maloof, A.C., 2010. Testing models for post-glacial 'cap dolostone' deposition: Nuccaleena Formation, South Australia. Earth Planet. Sci. Lett. 296, 165–180.
Schoene, B., Bowring, S.A., 2006. U-Pb systematics of the McClure Mountain syenite: thermochronological constraints on the age of the 40Ar/39Ar standard MMhb. Contrib. Miner. Petrol. 151, 615–630.
Scott, T.B., Allen, G.C., Heard, P.J., Randell, M.G., 2005. Reduction of U(VI) to U(IV) on the surface of magnetite. Geochim. Cosmochim. Acta 69, 5639–5646.
Skirrow, R.G., Bastrakov, E.N., Baroncii, K., Fraser, G.L., Creaser, R.A., Fanning, C.M., Raymond, O.L., Davidson, G.J., 2007. Timing of iron oxide Cu-Au-(U) hydrothermal activity and Nd isotope constraints on metal sources in the Gawler craton, South Australia. Econ. Geol. 102, 1441–1470.
Sláma, J., Košler, J., 2012. Effects of sampling and mineral separation on accuracy of detrital zircon studies, Geochem. Geophys. Geosystems, 13, 17.
Sláma, J., Košler, J., Condon, D.J., Crowley, J.L., Gerdes, A., Hanchar, J.M., Horstwood, M.S.A., Morris, G.A., Nasdala, L., Norberg, N., Schaltegger, U., Schoene, B., Tubrett, M.N., Whitehouse, M.J., 2008. Plešovice zircon – a new natural reference material for U-Pb and Hf isotopic microanalysis. Chem. Geol. 249, 1–35.
Thompson, J., Meffre, S., Maas, R., Kamenetsky, V., Kamenetsky, M., Goemann, K., Ehrig, K., Danyushevsky, L., 2016. Matrix effects in Pb/U measurements during LA-ICP-MS analysis of the mineral apatite. J. Anal. At. Spectrosc. 31, 1206–1215.
Trueman, N.A., 1986, Lead-uranium systematics of the Olympic Dam deposit and Stuart Shelf mineralization: Summary report of U-REE mineralization, Adelaide, Australia: Western Mining Corp., internal memo, XPSA86/1, 13 January 1986, 7 p.
Wiedenbeck, M., Alle, P., Corfu, F., Griffin, W.L., Meier, M., Oberli, F., Von Quadt, A., Roddick, J.C., Spiegel, W., 1995. Three natural zircon standards for U-Th-Pb, Lu-Hf, trace element and REE analysis. Geostandards Newsl. 19, 1–23.
Williams, G.E., 1998. Late Neoproterozoic periglacial aeolian sand sheet, Stuart Shelf, South Australia. Aust. J. Earth Sci. 45, 733–741.
Wingate, M.T.D., Campbell, I.H., Compston, W., Gibson, G.M., 1998. Ion microprobe U-Pb ages for Neoproterozoic basaltic magmatism in south-central Australia and implications for the breakup of Rodinia. Precambr. Res. 87, 135–159.
Yeo, G.M., Potter, E.G., 2010, Review of reducing mechanisms potentially involved in the formation unconformity-type uranium deposits and their relevance to exploration, Summary of investigations 2010, Volume 2, Saskatchewan Geological Survey, Sask. Ministry of Energy and Resources, p. 13.

View publication stats